Use of the $(e,e'n)$ reaction to study the giant multipole resonances in ^{116}Sn

R. A. Miskimen,* E. A. Ammons, J. D. T. Arruda-Neto,† G. O. Bolme,‡ L. S. Cardman, P. L. Cole,§
J. R. Deininger, S. M. Dolfini, A. J. Linzey, J. B. Mandeville, B. L. Miller,** P. E. Mueller, C. N. Papanicolas,
A. Serdarevič, and S. E. Williamson
Nuclear Physics Laboratory and Department of Physics, University of Illinois at Urbana-Champaign, Champaign, Illinois 61820
(Received 24 September 1990)

The giant multipole resonances in ^{116}Sn have been studied using the $(e,e'n)$ reaction. Data were taken at effective momentum transfers of 0.37, 0.45, and 0.55 fm^{-1} and a multipole analysis of the data was performed. The inferred multipole strength functions identify the $E2$ and $E0$ resonances as distinct peaks at 12.2 and 17.9 MeV, respectively. The energy-weighted sum-rule strengths for the $E2$ and $E0$ resonances, obtained using a Lorentzian fit to the data, are 34±13% and 93±37%. When compared with results from alpha scattering and pion scattering the sum-rule strengths exhibit approximate agreement, but the $E0$ strength identified in this measurement lies at higher excitation energy, consistent with the trend observed in heavier nuclei. The $(e,e'n)$ data are compared with a continuum random phase approximation (RPA) calculation of the $E2$ and $E0$ strengths, and with an open-shell RPA calculation of the $E2$ strength. Both calculations disagree with the data in the region of the $E2$ resonance.

I. INTRODUCTION

The giant multipole resonances (GMR) are found in all but the lightest nuclei and they are of fundamental importance in understanding the collective behavior of the nuclear many-body problem and the bulk properties of nuclear matter.[1] With the exception of the isovector giant dipole resonance ($E1$), relatively little is known about the GMR except for the systematics of excitation energies and decay widths. Experimental progress has been slow because the GMR are in the continuum and have substantial widths and, consequently, overlap one another.

Hadron-scattering and single-arm electron-scattering experiments have provided most of the information about the giant monopole and quadrupole resonances ($E0$ and $E2$). Hadron scattering is sensitive to isospin and can, in principle, disentangle $E0$ from $E2$ strength. In electron scattering the interaction is electromagnetic and, in principle, understood, and the kinematics can be chosen to select longitudinal charge scattering or transverse magnetic scattering. Nevertheless, the analysis of the hadronic and electromagnetic experiments are difficult and susceptible to systematic error. The hadron-scattering experiments must contend with nonresonant background that need to be subtracted from the data, and the excitation of many multipolarities, which make multipole decomposition difficult. In single-arm electron scattering, (e,e'), reliably subtracting the elastic radiative tail from beneath the giant resonances is problematic and reduces the accuracy of the probe. The problem of the elastic radiative tail in electron scattering was first avoided in $(e,e'p)$ coincidence experiments. These experiments remove the contribution of the elastic radiative tail at the detection stage. The suppression of charged-particle decay by the nuclear Coulomb barrier limits the use of the $(e,e'p)$ reaction to the study of GMR in primarily light nuclei. Given that the GMR are collective excitations, it can be argued that the GMR are best studied in heavy nuclei. Recently the $(e,e'n)$ reaction has been developed for giant resonance studies in heavy nuclei.[2,3] In heavy nuclei the branching ratio for neutron decay, Γ_n/Γ, is approximately unity. The work reported here on ^{116}Sn is part of a systematic study of giant resonances in heavy nuclei using the $(e,e'n)$ reaction.

Our experimental program began with a study of the GMR in ^{208}Pb and, for several reasons, ^{116}Sn was chosen as the next case to consider. First, (γ,n) data[4] are available on ^{116}Sn, providing an accurate estimate of the $E1$ multipole content in the data. There have also been numerous hadron-scattering experiments on Sn isotopes, so that comparisons can be made with other experiments.[5–8] In particular, Ullmann *et al.* have reported an anomalous ratio of π^+ to π^- scattering on ^{118}Sn, which they have interpreted as indicating a large isovector component in the isoscalar quadrupole resonance. Evidence for this could be seen in an $(e,e'n)$ experiment through a low $E2$ sum-rule fraction; Ullmann *et al.* report 25% for this sum rule. Because the Sn isotopes are medium-weight nuclei, the $E0$ centroid energy is an important data point for analyses that determine the compressibility of nuclear matter, providing additional input for the difficult task of isolating surface from bulk compressibility. For heavy nuclei, the centroid energy of the $E0$ resonance has been found to be quite close to the $80A^{-1/3}$ MeV value of the hydrodynamic model. For medium-weight nuclei, the centroid energies have been found to deviate increasingly from this value, suggesting the importance of surface effects.[9] Finally, the Sn isotopes are semimagic with a closed proton shell at $Z=50$, which

simplifies calculations and makes comparisons with experiments more reliable.

Compared to other types of coincidence experiments, the technical problems in an $(e,e'n)$ giant resonance experiment are especially severe. One reason is that the neutron detector must have adequate detection efficiency for neutron energies as low as 1 MeV. This increases the sensitivity of the neutron detector to γ rays from the target, giving a high singles rate in the detector and a high accidental coincidence rate. Another problem is that the neutron energy is measured with the time-of-flight (TOF) technique, so the true peak in the TOF spectrum is not a sharp peak, but may be many tens of ns wide. Unfortunately, the number of accidental coincidences that must be accepted also increases with the width of the peak. Finally, the detection efficiencies for neutrons detectors are low and not easily measured, and therefore introduce significant systematic error into the experimental results. This paper reports in depth on an $(e,e'n)$ experiment and the relevant experimental technique and method used to perform a study of the $E2$ and $E0$ resonances.

To facilitate comparison with theory, a multipole decomposition analysis is performed to separate the $E2$ and $E0$ strength from $E1$ strength. Despite significant statistical and nonstatistical uncertainties, the data presented here show clear evidence for resonance strength in the excitation region from 10 to 20 MeV. Furthermore, the data show evidence that the resonance strength is localized at approximately 12.2- and 17.9-MeV excitation. This strength is identified as the $E2$ and $E0$ resonances, respectively. The data are compared with results from (α,α') experiments[6,7] and a (π,π') experiment.[8] The resonance strengths inferred from these experiments are in approximate agreement, although the excitation energy of the $E0$ resonance obtained from the $(e,e'n)$ experiment is higher than that obtained from the hadron-scattering experiments. The excitation energy of the $E0$ resonance is close to the $80A^{-1/3}$ MeV rule observed in heavier nuclei. This result does not agree with observations from other experiments on medium-weight nuclei of a significantly lower $E0$ energy. The $(e,e'n)$ data are also compared with the results of a continuum RPA calculation for ^{132}Sn and an open-shell RPA calculation for ^{118}Sn. In the region of the $E2$ resonance, both calculations predict approximately twice the strength seen in the $(e,e'n)$ data. We conclude that more theoretical work is needed on Sn.

The rest of this paper is organized in the following way: the experimental procedure and data analysis are described in Sec. II; the multipole analysis of the data is described in Sec. III; the results from this experiment are compared with other experiments and theory in Sec. IV; and finally, the results are summarized and discussed in Sec. V.

II. EXPERIMENTAL METHOD AND DATA ANALYSIS

A. Experimental apparatus

The experiment was performed using the electron-scattering facility of the Nuclear Physics Laboratory at the University of Illinois at Urbana-Champaign (NPL). 100% duty factor electron beams with energies of up to 100 MeV and currents of up to 200 nA were incident on a 51.85-mg/cm^2 isotopically enriched ^{116}Sn target. Scattered electrons were detected in the NPL 200-MeV/c magnetic spectrometer with solid angle of 5.0 msr, a momentum acceptance of 6%, and a momentum resolution of $\delta p/p$ of 10^{-3}. Electron events were identified by a fourfold coincidence of a vertical drift chamber, two scintillators, and a Čerenkov counter. The product of the spectrometer solid angle and its electron detection efficiency was determined by a comparison between measured ^{116}Sn elastic-scattering cross sections and a phase-shift calculation of the elastic-scattering cross section using the known ground-state charge density;[10] it was always found to be greater than 90% of the geometric solid angle. Data for $(e,e'n)$ were taken at three different kinematic settings: $E=68.3$ MeV and $\theta_e=55°$; $E=68.4$ MeV and $\theta_e=71.2°$; and $E=99.4$ MeV and $\theta_e=59°$. Here E is the electron beam energy and θ_e is the electron-scattering angle. The corresponding effective momentum transfers were $q_{\rm eff}=0.37$, 0.45, and 0.55 fm^{-1}, respectively. Cross sections were measured for excitation energies from 10 to 20 MeV.

Two neutron detectors were employed for the experiment. The neutron detectors were cylindrical glass flasks 28 cm in diameter and 5 cm deep filled with NE-213 liquid scintillant. Three Amperex XP-2041 photomultipliers, each 13 cm in diameter, were coupled optically to the flask to detect light. The two neutron detectors were placed in the electron-scattering plane with one approximately antiparallel to the momentum-transfer direction and the other perpendicular to it. The neutron flight path was set at 1.0 m for each detector and each subtended a solid angle of 64 msr. To shield against photons, the neutron detector was surrounded on all sides by 10 cm of lead, except at the front of the detector where there was 5 cm of lead. The 5 cm of lead in front of the detector was essential for reducing photon backgrounds from the target. To shield against background neutrons from the room, the lead-encased detectors were surrounded on all sides except the front by 20 cm of borated paraffin. Borated paraffin collimators were placed in the gap between the front of the detectors and the scattering chamber to complete the shielding.

To meet the specific requirements of the neutron detector logic, the tube base was designed so as to provide one anode signal and two dynode signals. A neutron pretrigger was generated by passively inverting a signal from the 14th dynode on each tube, passing it through a leading-edge discriminator, and forming a two-out-of-three (majority) coincidence between the tubes of a neutron detector. To maximize the efficiency of the neutron detection, the discriminator thresholds were set very low, well into the tube noise; the majority coincidence requirement eliminated noise from the pretrigger. The anode signals from the three tubes were averaged with an emitter follower circuit, which provided a threefold analog output that was sent to a constant-fraction discriminator (CFD) and two charge-sensitive analog-to-digital converter ADC's. The timing signal from the CFD was placed

in coincidence with the pretrigger to eliminate noise signals and then used as a trigger to the coincidence-processing electronics.[11] During data taking, typical singles rates in the neutron detectors were 50 kHz. Because of the high accidental coincidence rates in this experiment, it was essential that the relative timing between the neutron detectors and the electron spectrometer be established before data taking began. This calibration was performed using a PuBe source.

B. Photon-neutron discrimination

The number of photons observed in the neutron detectors while taking data typically exceeded the number of neutrons by an order of magnitude, greatly increasing the accidental coincidence rate. To log data with an acceptable trues-to-accidentals ratio and at acceptable rates, it was necessary to discriminate against photon events both on line (while taking data) and off line (in the data analysis). This was done by using both analog and digital pulse-shape discrimination (PSD) techniques. For on-line PSD, the signal from dynode 13 from each of the three photomultiplier tube bases was passively added in an integrating preamplifier with a 5-μs time constant. The preamplifier signal was then used as the input for a fast analog PSD module designed and constructed[2] at the University of Illinois. In order to maintain neutron detection efficiency as high as possible, the PSD cut was adjusted so that approximately 10% of the photon events would remain in the data after the cut. The remaining photons in the data were eliminated off line by using digital pulse-shape discrimination. In this procedure, one charge-sensitive ADC was gated to measure the charge in the first 40 ns of the anode pulse, and a second ADC was gated to measure the charge in the next 300 ns of the pulse. In a contour plot of early gate charge versus late gate charge, the remaining photons were identified and removed from the data; an example of this is shown in Fig. 1. In addition, an energy threshold was set for the detector based on the charge in the early gated ADC; this threshold was approximately 80-keV equivalent photon energy.

Absolute flight times in the TOF spectra were calibrated by reversing the digital pulse-shape discrimination procedure to accept photon events rather than neutron events. When this was done, a peak was observed in the TOF spectra corresponding to the measurement of coincident bremsstrahlung photons from the $(e,e'\gamma)$ reaction. The "zero" time can be inferred from the location of this peak, the known flight path, and the velocity of light. The coincidence-resolving time between the neutron detectors and the electron spectrometer can also be determined by using this photon peak; it was less than 2 ns FWHM. This resolving time is consistent with the 5-cm depth of the neutron detectors.

After the photon cuts were made, substantial numbers of accidental events remained in the neutron TOF spectra; an example is shown in Fig. 2. The accidental coincidentals were caused primarily by the high neutron singles rate from the target. The accidentals were subtracted from the coincident yield by using those portions of the TOF spectrum that were known from energy considerations to contain only accidental events. To provide clean data for this subtraction, a 200-ns-wide coincidence window was used for data acquisition even though the base width of the neutron TOF peak was only 50 ns.

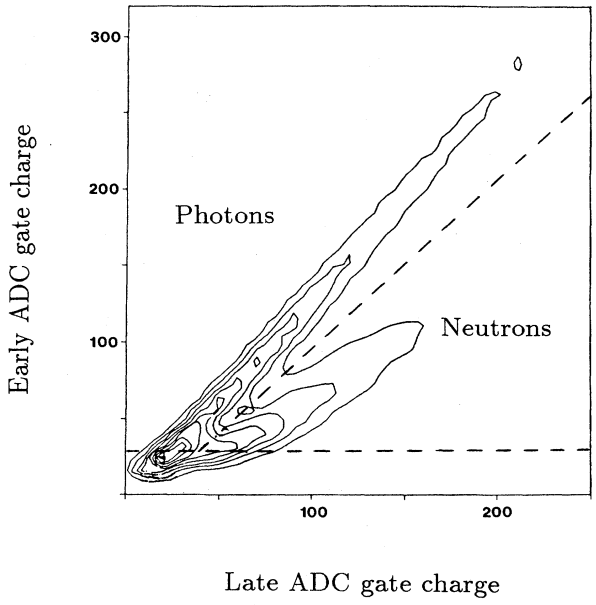

FIG. 1. Digital pulse-shape discrimination. The horizontal axis is the late gate charge, and the vertical axis is the early gate charge collected in the ADC. The dashed lines show the cuts made for photon-neutron discrimination.

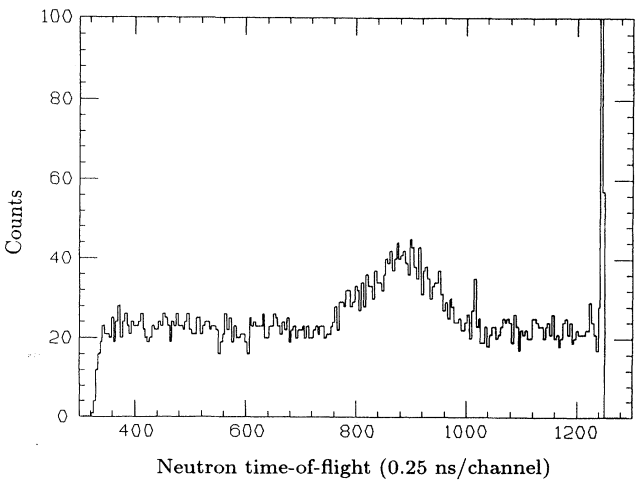

FIG. 2. Neutron time-of-flight spectrum for $E=99.4$ MeV and $\theta_e=59°$. The units on the horizontal axis are 0.25 ns per channel. The events in this spectrum have passed analog and digital pulse-shape discrimination.

C. Efficiency calibration

The efficiencies of the neutron detectors were calibrated both before and after the experiment. The calibration was done with the detectors and the surrounding shielding in the same configuration as was used for the experiment to eliminate sensitivity to rescattering in the shielding. The procedure used the coincident fission fragments and neutrons from a ^{252}Cf source. The efficiency was calibrated by mounting the ^{252}Cf source close to the face of a solid-state detector and then mounting the detector and source in the target chamber at the scattering center. The solid-state detector was sensitive only to highly ionizing fission fragments, not neutrons or gamma rays. Neutrons emitted in the fission event were detected in the neutron detectors. To calibrate the detectors, the fission signal from the solid-state detector was substituted for the electron identification signal from the spectrometer in the coincidence-processing electronics. The electronics were started by a fission event in the solid-state detector, and stopped by a neutron event in one of the neutron detectors. To obtain the detector efficiency as a function of TOF, the known[12] energy distribution of neutrons emitted in the spontaneous fission of ^{252}Cf was convoluted with the measured time response of the neutron detectors and then compared with the measured TOF distribution. The ^{252}Cf data were analyzed using the same analog and digital pulse-shape discrimination cuts as were applied to the $(e,e'n)$ data.

Because of the supports necessary to secure the ^{252}Cf source, the solid-angle acceptance for fission fragments of the solid-state detector was 20% of 2π. During calibration, the angle of the source-detector assembly relative to the neutron detectors was changed to check for anisotropies in the neutron angular distribution, strong anisotropies were observed. Figure 3 shows the typical coincident-neutron yield per fission event as a function of the detector angle. The angle is measured relative to the vector normal to the surface of the solid-state detector. These anisotropies were caused by the limited solid-angle coverage of the solid-state detector for fission fragments. Fission fragments resulting from the spontaneous fission of ^{252}Cf move at high velocity and, because of this, the laboratory angular distribution for nonprompt neutrons (those emitted from a fragment) is anisotropic and peaked in the direction of the moving fragment. If the solid-angle acceptance for fission fragments in the solid-state detector had approached 2π, then the measured neutron angular distribution would have been isotropic.[13] This is because the solid-state detector would have averaged over all fragment directions, including neutrons emitted from fragments moving away from the solid-state detector because the sister fragment would recoil into the detector. Since it was not practical to build a detector with 2π fission acceptance, or to have a ^{252}Cf source deposited on the surface of a solid-state detector, the neutron angular distribution was measured as a function of the angle θ between the normal vector to the solid-state detector and the line between the solid-state detector and the center of the neutron detectors, and the neutron energy E_n. Then the angular distribution was averaged over a 4π solid angle to obtain a detector efficiency that is a function only of E_n. The solid-angle averaging was performed by fitting an expression proportional to

$$1+\alpha(E_n)\cos^2(\theta) \tag{1}$$

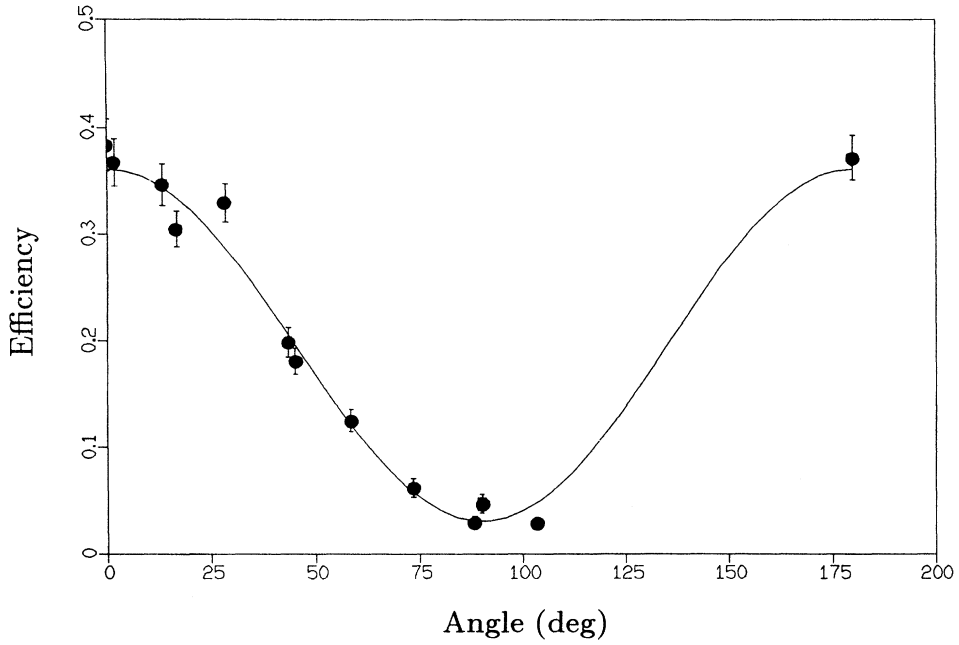

FIG. 3. Measured neutron angular distribution in the ^{252}Cf calibration procedure. The relative efficiency for neutron detection per fission event is plotted as a function of the angle between the neutron detector and the normal vector to the surface of the solid-state detector.

to the measured neutron angular distribution. In this expression, $\alpha(E_n)$ is a fitted parameter that depends on neutron energy. In Eq. (1), higher-order terms in $\cos^2(\theta)$ were found not to be important; the energy dependence of $\alpha(E_n)$ was strong, results from the fit showed that $\alpha(E_n)$ varied from 1.55 ± 0.05 at $0.5<E_n<1.5$ MeV, to 10.8 ± 1.2 at $5.5<E_n<6.5$ MeV. To obtain the detector efficiency, the neutron TOF distribution was averaged over all angles and then compared with the standard ^{252}Cf neutron velocity distribution convoluted with the neutron detector time response. Figure 4 shows a typical neutron detector efficiency obtained from this procedure. The efficiency peaks at 23% at 2 MeV and then falls rapidly with decreasing energy to 0% efficiency at 0.5 MeV. The sharp cutoff at low energies is caused by the cut on low pulse heights in the ADC. At energies above 2 MeV, the efficiency falls off gradually to approximately 10% efficiency at 10 MeV.

The objective of the data analysis was to obtain equivalent single-arm electron-scattering cross sections from the $(e,e'n)$ data missing, of course, the elastic radiative tail. The first step was to correct for neutron detector inefficiencies. This was done by calculating an acceptance for each detector as a function of nuclear excitation energy, and then dividing the uncorrected yield by this acceptance. The acceptance was defined as

$$A(\omega)=\frac{N_T(\omega)}{N_C(\omega)}\ , \tag{2}$$

where $A(\omega)$ is the detector acceptance at excitation energy ω, $N_T(\omega)$ is the number of true events (accidental coincidences having been removed), and $N_C(\omega)$ is the number of true events corrected for inefficiencies. The number of true events was calculated by summing the neutron TOF spectra using a typical bin width in excitation energy of 2 MeV. To correct for detector inefficiencies, the neutron TOF spectra were first divided by the neutron detector efficiency. Then, to correct for neutrons with energies below the detection threshold, a statistical decay model was extrapolated to the low-energy portion of the efficiency-corrected neutron spectra. The neutron spectra were parametrized for each range of nuclear excitation by the Maxwellian distribution

$$N(E_n)=N_C E_n \frac{e^{-E_n/kT}}{(kT)^2}\ , \tag{3}$$

where $N(E_n)$ is the neutron energy spectrum, and N_C and kT were fitted to the data. Generally, only 20% of the events were found to be below the detection threshold, therefore, the use of the Maxwell distribution as an approximation to the neutron energy spectrum did not present a serious limitation to the analysis. Over most of the excitation region studied, the detector acceptance was typically 0.16 and kT was approximately 0.7 MeV. Figure 5 shows a logarithmic plot of $N(E_n)/E_n$ as a function of E_n and the fitted energy distribution. Note that the $1/E_n$ weighting of the data in Fig. 5 inflates the relative importance of the neutron spectrum at low energies.

The two neutron detectors were oriented approximately antiparallel and perpendicular to the momentum-transfer direction. Comparisons of the corrected yields in the two neutron detectors showed that they were equal, within statistical errors, over most of the excitation region covered. This justified the assumption that the neu-

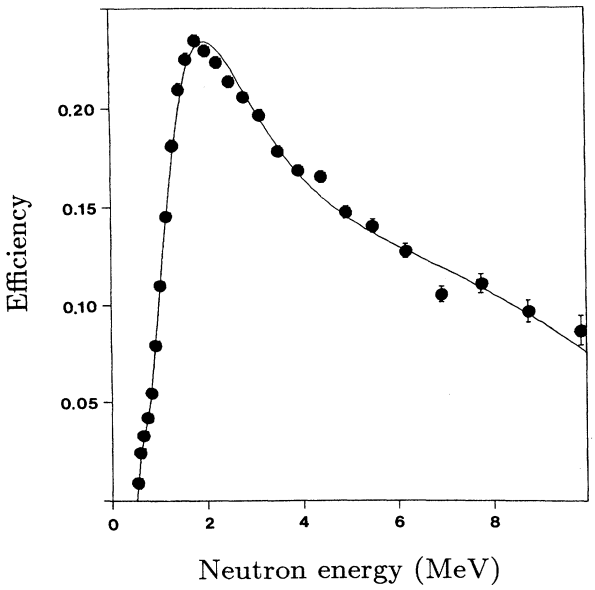

FIG. 4. Neutron detector efficiency as a function of neutron energy. The smooth curve is a polynomial fit to the data points.

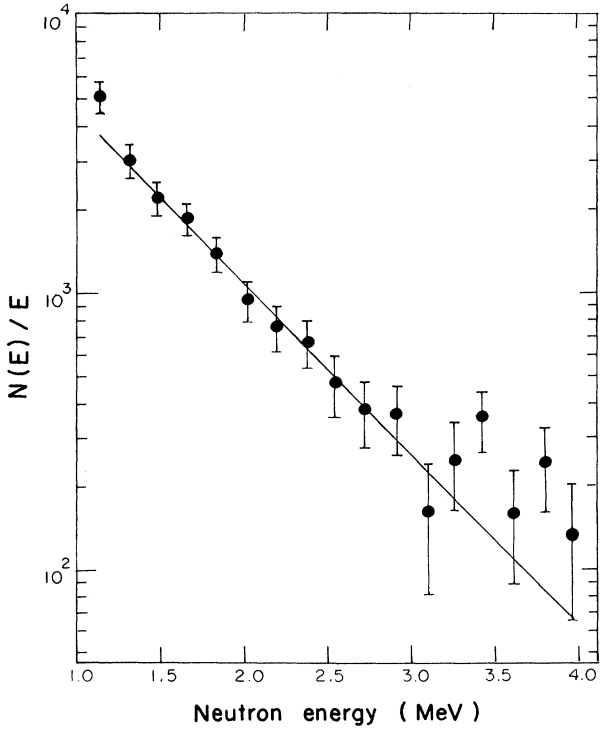

FIG. 5. Neutron energy spectrum. $N(E_n)$ is the number of neutrons per unit energy; E_n is the neutron energy. The straight line is a fit to a statistical decay model.

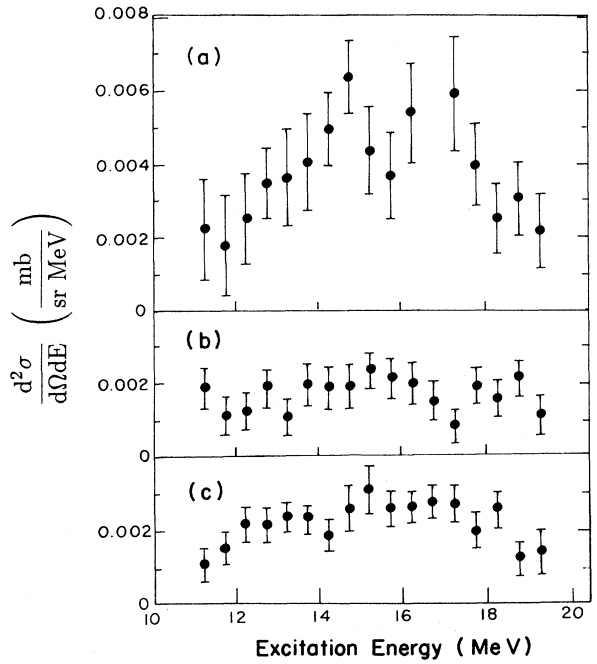

FIG. 6. $(e,e'n)$ differential cross sections averaged over neutron solid angle for (a) $E=68.3$ MeV and $\theta_e=55°$, $q=0.37$ fm^{-1}, (b) $E=68.4$ MeV and $\theta_e=71.2°$, $q=0.45$ fm^{-1}, and (c) $E=99.4$ MeV and $\theta_e=59°$, $q=0.55$ fm^{-1}. The units are mb/sr MeV.

tron decay is isotropic. Using the assumption that the branching ratio for neutron decay for ^{116}Sn for these excitations is approximately 100%, the $(e,e'n)$ cross sections were averaged and integrated over a neutron solid angle to obtain equivalent single-arm electron-scattering cross sections.

Radiative corrections were made on the data by calculating,[14] for a given excitation energy bin, the amount of cross section falling into successively higher bins because of radiative effects. Starting from the lowest to the highest excitation energies, this cross section was successively stripped away from higher excitation energy bins. The resulting electron-scattering cross sections for the three different momentum transfers are shown in Fig. 6.

D. Multipole analysis

The kinematics of this experiment ($q_{\rm eff}\leq 0.55$ fm^{-1}, $\theta_e<71.2°$, $\omega<20$ MeV) were chosen to emphasize the longitudinal excitation of the $E0$, $E1$, and $E2$ giant resonances. With these kinematics, the $E3$ contribution to the cross section is anticipated to be insignificant.[2] For comparison with theory and other experiments it was useful to separate the contribution of the isovector $E1$ resonance from the contributions of the $E2$ and $E0$ resonances. This was done through a multipole analysis[15,16] in which the $E0$, $E1$, and $E2$ transition charge densities were described by the Tassie form.[17] It was not possible to separate $E0$ from $E2$ in such a multipole analysis because, for low-q values, the q dependence of these $E0$ and $E2$ form factors are identical and the total transition form factor is sensitive to a weighted sum of $dB(E2)/d\omega$ and $dB(E0)/d\omega$. Using the plane-wave Born approximation (PWBA) it can be shown that the relative weighting is given exactly by

$$\frac{dB(E2)}{d\omega}+\frac{25}{16\pi}\frac{dB(E0)}{d\omega}\ . \tag{4}$$

In the distorted-wave Born approximation (DWBA) this relation is approximately valid.

For simplicity, the transition charge density for each multipole was assumed to be independent of excitation energy. This approximation is supported by a RPA calculation by Wambach and Co for ^{208}Pb in which the transition charge form factors for the $E0$, $E1$, and $E2$ resonances were calculated as a function of excitation energy.[2] Their calculation showed that, at low momentum transfer, the transition charge form factors are approximately independent of excitation energy, and that the transition radii of the $E0$, $E1$, and $E2$ resonances are approximately equal to the ground-state radius. Therefore, in the multipole analysis it was assumed that the half-density radius parameter of the Tassie model satisfies

$$c_{\rm tr}(E1)=c_{\rm tr}(E2)=c_{\rm g.s.}\ . \tag{5}$$

The parameter $c_{\rm g.s.}$ and the diffuseness parameter $z_{\rm g.s.}$ were obtained by fitting the surface region of the ground-state charge density[10] with a Fermi shape; the values obtained were $c_{\rm g.s.}=5.28$ fm and $z_{\rm g.s.}=0.58$ fm. Using the Tassie-model transition density, electron-scattering cross sections were calculated as a function of excitation energy using DWBA. Values of $dB(E1)/d\omega$ and $dB(E2)/d\omega$ were then fitted to the (γ,n) (Ref. 4) and $(e,e'n)$ data. In the multipole analysis, the $E1$ strength was strongly constrained at the $q=\omega$ point by the (γ,n) data, which was dominantly $E1$.

Figure 7 shows the resonance strength inferred from the multipole decomposition analysis. The uncertainties shown in the figure include statistical and nonstatistical errors. The nonstatistical error results from fitting the data to model-dependent form factors that may not describe the momentum transfer and excitation energy behavior of the data reasonably. Evidence for this was found in the average chi square per degree of freedom in the multipole analysis; averaged over the 17 excitation energy bins from 11.25 to 19.75 MeV, this value was 1.58. For two degrees of freedom the probability of observing a chi square larger than this is only 21% if the form factors correctly describe the data. Additional systematic error (not shown in the figure) is dominated by two main sources. The first source results from uncertainties in neutron detection efficiency and model error in the multipole analysis. The latter effect was tested by varying $c_{\rm tr}(E1)$ and $c_{\rm tr}(E2)$ within reasonable limits ($\pm 10\%$) and finding the change in $dB(E2)/d\omega$. The combined error in the strength from uncertainties in neutron detector efficiencies and model error in the multipole analysis is estimated to be approximately $\pm 30\%$. The other major source of systematic error derives from the absolute normalization of the (γ,n) data. To study the effect of the (γ,n) systematic error on the multipole analysis, the

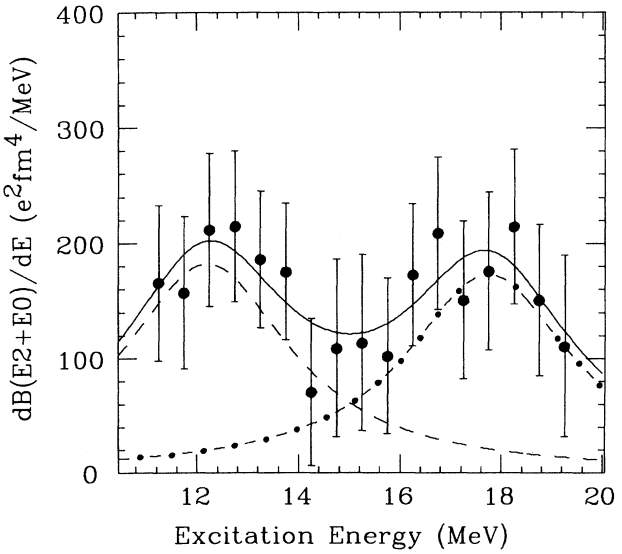

FIG. 7. Multipole strength versus nuclear excitation energy for ^{116}Sn. The data points are the results of this experiment. The systematic error is not shown. The dashed and dash-dotted curves show a Lorentzian fit to the data, and the solid curve shows the sum of the two Lorentzians.

(γ,n) data were shifted up and down by an amount given by the systematic error in that experiment, and then used in the multipole analysis. The effect on the resonance strength was ±20%. Combining these two sources of error in quadrature gives a total systematic error of approximately ±36%. Clearly, this measurement has significant uncertainties and would benefit from the future development of large solid-angle and large momentum-acceptance electron spectrometers used in conjunction with medium-energy 100% duty-factor electron beams. The measurement would also benefit from improved (γ,n) data.

Despite the significant uncertainties in the data, the experiment clearly shows resonant strength in the excitation region from 10 to 20 MeV. Furthermore, the data suggest the resonant strength is maximized at excitation energies of approximately 12 and 17.5 MeV. Systematic trends[18] in giant resonance data support the identification of these regions as $E2$ and $E0$ resonances. The statistical significance of the dip in the resonance strength at approximately 15-MeV excitation was tested by adjusting the strength to a constant value from 11.25 to 19.75 MeV and then calculating chi square. For this test, the constant strength used, 152 e^2 fm^4/MeV, was chosen because it gave the minimum chi-square fit to the data. Using a constant multipole strength caused the average chi square per degree of freedom to increase from 1.58 to 1.87. Assuming that this multipole model correctly describes the ω dependence of the data, the probability for observing a larger chi square drops from 21 to 16 %. The $(e,e'n)$ data presented here show evidence that the $E2$ and $E0$ strength is resolved. The peak-and-valley structure seen in the ^{116}Sn $(e,e'n)$ data is analogous to the situation in ^{208}Pb, where the $E2$ and $E0$ were resolved in an earlier $(e,e'n)$ experiment.[2]

Summing the strength from 11.25 to 15 MeV gives 20.6±2.8±7.4 % of the $E2$ energy-weighted sum rule, and from 15 to 19.75 gives 61±8.8±22 % of the $E0$ energy-weighted sum rule, where the first uncertainty contains the statistical and nonstatistical errors of the multipole analysis, and the second uncertainty is the systematic error. To gauge the measured multipole strength while including strength outside the excitation range of the experiment, the $(e,e'n)$ data were also fitted with two Lorentzians. In the fitting procedure, the excitation and strength of the Lorentzians were varied, but the widths of both line shapes were fixed at 4.0 MeV to give a better constraint on the fit. Systematic trends in giant resonance data have suggested that 4 MeV is the approximate width of the $E2$ and $E0$ resonances in this mass region.[18] The fitted positions and energy-weighted sum-rule strengths for the Lorentzians are 12.2±0.7 MeV and 34±6±12 % for the $E2$, and 17.9±0.9 MeV and 93±17±33 % for the $E0$. Combining the statistical and nonstatistical errors in quadrature with the systematic error gives 34±13 % and 93±37 % for the $E2$ and $E0$ energy-weighted sum rules, respectively. The Lorentzian fits to the data are shown in Fig. 7.

III. COMPARISON WITH OTHER EXPERIMENTS AND THEORY

Figures 8 and 9 compare the results of this experiment with the alpha-scattering experiment of Bonin *et al.*[6] on ^{116}Sn and the pion-scattering experiment of Ullmann *et al.*[8] on ^{118}Sn, respectively. The upper half of each of these figures shows the experimental error bands for the combined $E0$ and $E2$ strength inferred from the alpha- and pion-scattering experiments, while the lower halves of the figures show the separate contributions from $E0$ and $E2$ as well as the combined strength. The relative weighting of the combined $E2$ and $E0$ strength used to produce the curves in these figures is given by Eq. (4). The error bands were derived by combining the $E0$ and $E2$ uncertainties in quadrature. The figures show that the quality of the $(e,e'n)$ measurement is comparable to what has been achieved using hadronic probes. They also show that the $(e,e'n)$ data and the alpha- and pion-scattering data disagree on the shape of the resonance strength. The $(e,e'n)$ data show evidence for two peaks, centered at 12.2±0.7 and 17.9±0.9 MeV, while the alpha- and pion-scattering data exhibit a single peak. The difference in shapes is due primarily to the position of the $E0$ resonance; the excitation energy of the $E0$ strength identified in this experiment is higher than that identified in the hadron-scattering experiments. The alpha- and pion-scattering experiments found $E0$ strength centered at 15.9±0.4 and 15.5 MeV, respectively, which also agrees with another (α,α') result by Sharma *et al.*[7] of 15.69±0.16 MeV for the $E0$ centroid. The sum-rule strengths resulting from this analysis are in approximate agreement with those from the hadron-scattering experiments. Bonin *et al.* found 47±12 % and 25±13 % of the $E2$ and $E0$ sum rules, respectively, while

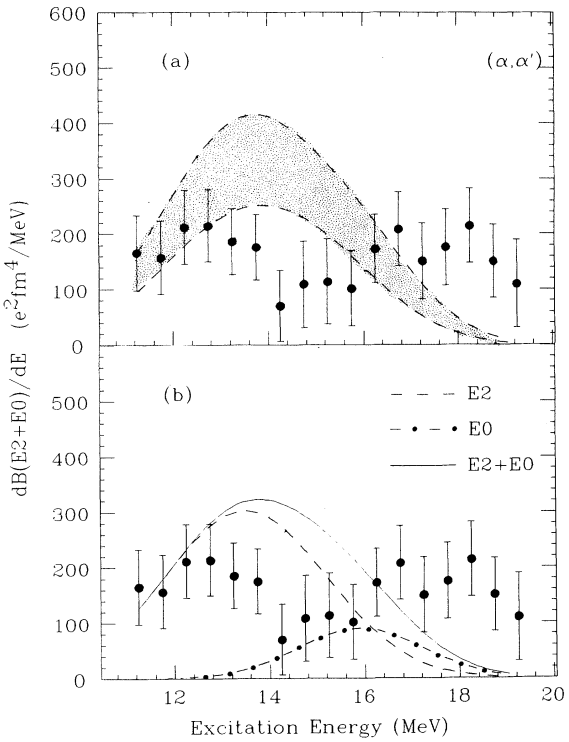

FIG. 8. (a) Multipole strength versus nuclear excitation energy compared with an alpha-scattering experiment (Ref. 6) on ^{116}Sn. The data points are the results of this experiment. The error band shows the results of the alpha-scattering experiment. (b) Same as for (a) except that the alpha-scattering results for the $E2$, $E0$, and combined $E2$-and-$E0$ are shown by the short-dashed, dash-dotted, and solid curves, respectively.

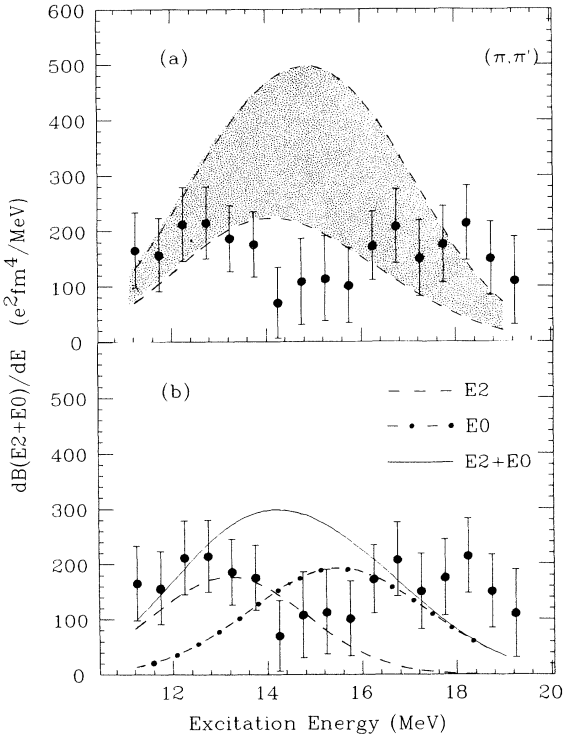

FIG. 9. (a) Same as for Fig. 8(a) except the comparison is for pion scattering (Ref. 8) on ^{118}Sn. (b) Same as for Fig. 8(b) except the comparison is for pion scattering (Ref. 8) on ^{118}Sn.

Ullmann *et al.* found 25±8 % and 74^{+84}_{-28} %. Sharma *et al.* found a significantly higher $E2$ sum-rule strength, 134±28 %, and an $E0$ sum-rule strength comparable to the other experiments, 101±22 %.

Figure 10 compares the data from this experiment with a recent continuum RPA calculation[19] for the $E2$ and $E0$ strength in ^{132}Sn. The calculation uses a phenomenological Woods-Saxon basis and a Landau-Migdal effective interaction. The effects of 2p-2h interactions are included using a semiempirical model.[20] The figure shows that the calculation fails to describe the data and, in the region of the $E2$ resonance, the theory is approximately twice as large as the experimental result. Given the poor agreement for the $E2$, it is interesting that the calculated position and strength of the $E0$ resonance agrees with the $E0$ strength inferred from the $(e,e'n)$ data.

The result of an open-shell RPA calculation for the $E2$ strength in ^{118}Sn by Brown *et al.*[21] is shown in Fig. 11. This calculation uses spherical Nilsson model configurations from $2d$-$\frac{5}{2}$ to $2f$-$\frac{7}{2}$ with a separable quadrupole particle-hole force. The parameters of the force were adjusted to place the 2_1^+ at its empirical energy, and an effective mass ratio of 0.75 was used to place the $E2$ resonance at an energy of $64A^{-1/3}$ MeV. This calculation used a realistic ratio of 1.04 for the ratio of neutron to proton rms radii. All significant $E2$ strength was found in five excitations from 9.5 to 13.2 MeV and was dominated by a single state at 13.2 MeV. The result shown in Fig. 11 was obtained by folding the state at 13.2 MeV with a Lorentzian of width 4 MeV. The $E2$

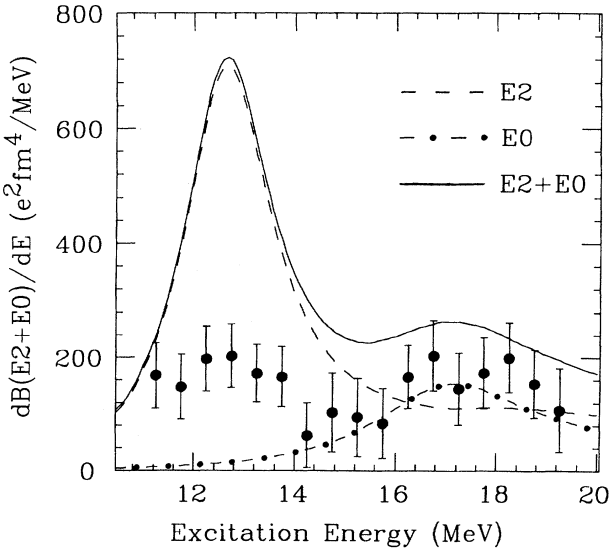

FIG. 10. Comparison of data and the results of a continuum RPA calculation for ^{132}Sn (Ref. 19). The dashed curve is the $E2$ strength, the dash-dotted curve the $E0$ strength, and the solid curve is the sum of $E2$ and $E0$.

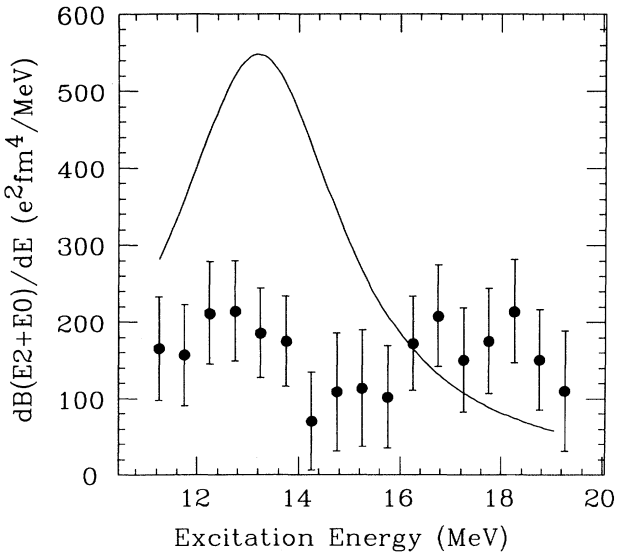

FIG. 11. Comparison of data and the results from an open-shell RPA calculation (Ref. 21) for ^{118}Sn that includes only the $E2$.

energy-weighted sum rule is strictly satisfied in the calculation. Comparison of theory with the $(e,e'n)$ data shows that the open-shell RPA calculation fails to describe the data. Like the continuum RPA calculation, the open-shell RPA calculation is more than twice as large as the $(e,e'n)$ data in the region of the $E2$ resonance. Note that the $E0$ resonance is not included in the theoretical curve.

IV. SUMMARY AND CONCLUSIONS

An $(e,e'n)$ experiment to study the giant multipole resonances in ^{116}Sn has been presented. Compared to many other types of coincidence experiments, the technical problems in an $(e,e'n)$ giant resonance experiment are severe but can be overcome. Because the neutron branching ratio is approximately unity for GMR decay in heavy nuclei, the $(e,e'n)$ reaction is particularly well suited for studying the GMR in heavy nuclei. The experimental techniques used in the measurement were discussed in detail. Despite significant statistical and nonstatistical uncertainties, the experiment clearly demonstrates resonance strength in the excitation region from 10 to 20 MeV, and the quality of the data (including statistical, nonstatistical, and systematic errors) is comparable to what has been achieved using hadronic probes.

The data show statistically significant evidence for two peaks in the sum of the $E0$ and $E2$ resonance strengths, centered at 12.2 and 17.9 MeV, which were identified as the $E2$ and $E0$ resonances, respectively. Using a Lorentzian fit, the first peak satisfies 34 ± 13 % of the $E2$ energy-weighted sum rule, and the second peak satisfies 93 ± 37 % of the $E\phi$ energy-weighted sum rule. The $(e,e'n)$ results were compared with alpha- and pion-scattering results, and there is approximate agreement between the sum-rule strengths observed in this experiment and in the hadron-scattering experiments, although the $E0$ strength identified in this experiment is at higher excitation energy. Given the different sensitivities of the hadron and electron probes to higher-resonance multipolarities, isospin, nonresonant backgrounds, and nuclear form factors, some disagreement should be expected.

The excitation energy of the $E0$ resonance is a subject of great interest because it can be related to the compressibility of nuclear matter. For heavy nuclei ($A > 160$), systematic trends indicate that the excitation energy of the $E0$ resonance is at approximatly $80A^{-1/3}$ MeV. For lighter nuclei the data are not expected to follow this rule because surface effects become more important as the mass number decreases. The systematics of lighter nuclei indicate a break in this trend in the direction of lower excitation energy[9] and, at $A \approx 60$, the data suggest that the $E2$ and $E0$ resonances might well coincide in excitation energy. To determine the compressibility of nuclear matter it is necessary to measure the excitation energy of the $E0$ resonance over a large range of A, so that bulk effects can be separated from surface effects. Therefore, the existence of this trend is a matter of some importance. Experimental data show the $E0$ sum-rule strengths decreasing almost linearly from about 100% depletion in $A > 160$ nuclei to about 10% in nuclei with $A \approx 60$.[9] This missing $E0$ sum-rule strength in light- and medium-weight nuclei may cast doubt on the validity of the $E0$ excitation energy systematics for light nuclei, since the missing sum-rule strength could well be at higher excitation energy. The $E0$ excitation energy inferred in this experiment, 17.9 ± 0.9 MeV, is actually higher than the empirical $80A^{-1/3}$ MeV rule, which gives 16.4 MeV for ^{116}Sn. Therefore, this measurement does not agree with observations from other experiments of a systematically lower $E0$ excitation energy in medium-weight nuclei.

The $(e,e'n)$ results were also compared with a continuum RPA calculation for ^{132}Sn and an open-shell RPA calculation for ^{118}Sn. For both calculations the agreement between experiment and theory was poor, especially in the region of the $E2$ resonance where the theories were twice as large as the data. Despite this fact, the $E0$ strength predicted by the continuum RPA calculation agrees quite well with the $E0$ strength inferred from the $(e,e'n)$ data. The situation in Sn contrasts greatly with ^{208}Pb, a doubly closed-shell nucleus, where the agreement between the $(e,e'n)$ data and RPA was excellent.[2] Clearly, more theoretical work is needed on nondoubly closed-shell nuclei such as Sn.

ACKNOWLEDGMENTS

The authors wish to thank J. Wambach for communicating the results of his calculations and for helpful comments. They also thank the operators and technicians of the MUSL-2 accelerator for providing the stable beam required for this experiment. This research was supported by the National Science Foundation under Grant NSF PHY 86-10493 and the Department of Energy under Grant DE-AC02-76ER02853.

*Present address: Department of Physics and Astronomy, University of Massachusetts, Amherst, Massachusetts 01003.
†Permanent address: Instituto de Física, Universidade de São Paulo, C.P. 20516, 01498 São Paulo, SP, Brazil.
‡Present address: Los Alamos National Laboratory, Los Alamos, New Mexico 87545.
§Present address: Naval Weapons Support Center, Crane, Indiana 47522.
**Present address: Kuch and Associated, Inc., Champaign, Illinois 61820.

[1]K. Goeke and J. Speth, Annu. Rev. Nucl. Part. Sci. **32**, 65 (1982).
[2]G. O. Bolme, L. S. Cardman, R. Doerfler, L. J. Koester, Jr., B. L. Miller, C. N. Papanicolas, H. Rothhaas, and S. E. Williamson, Phys. Rev. Lett. **61**, 1081 (1988).
[3]R. A. Miskimen, E. A. Ammons, J. D. T. Arruda-Neto, L. S. Cardman, P. L. Cole, J. R. Deininger, S. M. Dolfini, A. J. Linzey, J. B. Mandeville, B. L. Miller, P. E. Mueller, C. N. Papanicolas, A. Serdarevič, and S. E. Williamson, Phys. Lett. **236**, 251 (1990).
[4]A. Leprêtre, H. Beil, R. Bergère, P. Carlos, A. De Miniac, A. Veyssière, and K. Kernbach, Nucl. Phys. **A219**, 39 (1974).
[5]D. H. Youngblood, P. Bogucki, J. D. Bronson, U. Garg, Y. -W. Lui, and C. M. Rozsa, Phys. Rev. C **23**, 1997 (1981).
[6]B. Bonin, N. Alamanos, B. Berthier, G. Bruge, H. Faraggi, D. Legrand, J. C. Lugol, W. Mittig, L. Papineau, A. I. Yavin, D. K. Scott, M. Levine, J. Arvieux, L. Farvacque, and M. Buenerd, Nucl. Phys. **A430**, 349 (1984).
[7]M. M. Sharma, W. T. A. Borghols, S. Brandenburg, S. Crona, A. van der Woude, and M. N. Harakeh, Phys. Rev. C **38**, 2562 (1988).
[8]J. L. Ullmann, P. W. F. Alons, B. L. Clausen, J. J. Kraushaar, J. H. Mitchell, R. J. Peterson, R. A. Ristinen, R. L. Boudrie, N. S. P. King, C. L. Morris, J. N. Knudson, and E. F. Gibson, Phys. Rev. C **35**, 1099 (1987).
[9]A. van der Woude (unpublished).
[10]J. Cavedon, J. B. Bellicard, B. Frois, D. Goutte, M. Huet, P. Leconte, X. -H. Phan, and S. K. Platchkov, Phys. Lett. **118B**, 311 (1982).
[11]L. S. Cardman and C. N. Papanicolas, Argonne National Laboratory Report ANL/PHY-81-2, 1981 (unpublished).
[12]A. B. Smith and W. P. Poenitz, International Nuclear Data Committee Report INDC-36/LN, 1981.
[13]J. Cub, E. Finckh, K. Gebhardt, K. Geissdorfer, R. Lin, J. Strate, and H. Klein, Nucl. Instrum. Methods **A274**, 217 (1989).
[14]L. W. Mo and Y. S. Tsai, Rev. Mod. Phys. **41**, 205 (1969).
[15]M. Sasao and Y. Torizuka, Phys. Rev. C **15**, 217 (1977).
[16]D. H. Dowell, L. S. Cardman, P. Axel, G. Bolme, and S. E. Williamson, Phys. Rev. Lett. **49**, 113 (1982).
[17]L. J. Tassie, Aust. J. Phys. **9**, 407 (1956).
[18]F. E. Bertrand, Nucl. Phys. **A354**, 129c (1981).
[19]J. Wambach, private communication.
[20]R. D. Smith and J. Wambach, Phys. Rev. C **38**, 100 (1988).
[21]V. R. Brown, J. A. Carr, V. A. Madsen, and F. Petrovich, Phys. Rev. C **37**, 1537 (1988).